Available online at www.sciencedirect.com
SCIENCE DIRECT®
Journal of Nuclear Materials 329–333 (2004) 263–267
journal of nuclear materials
www.elsevier.com/locate/jnucmat

Thermal fatigue behaviour of different candidate structural materials: a comparative study ☆

G. Filacchioni *, E. Casagrande, U. De Angelis, G. De Santis, D. Ferrara, L. Pilloni

ENEA CR Casaccia, Technical-Scientific Unit for New Materials and Technologies, Technologies and Materials Qualification Section, New Materials Division, Via Anguillarese 301, S.M. di Galeria, Rome I-00060, Italy

Abstract

Some structural steels have been tested in a relevant thermal fatigue condition and their behaviour analysed to have a first indication about the effects of thermally induced cyclic loading on time to failure of a tokamak structural component. The behaviour of four reduced activation ferrous alloys has been compared to that of two 'conventional' high-medium strength martensitic steels and also to austenitic AISI 316 L(N). The conventional alloys have demonstrated their superiority, and an unexpected, quite good behaviour of the austenitic steel was also observed.

1. Introduction

The first wall and blanket components of a magnetic fusion reactor (MFR) will be subjected to a thermally induced cyclic loading owing to the pulsed plasma operation. These thermal stresses combine with other mechanical and shape/size constraints in such a way that this cyclic loading could constitute one of the limiting factors for a safe design of the machine.

In recent years, reduced activation martensitic ferrous alloys (RAMF) have been studied worldwide. Their unirradiated and post irradiation properties seem to indicate RAMF's suitability as structural materials in a fusion reactor [1–3]. Nevertheless, knowledge about the mechanical properties of these steels is incomplete; few data are available on fatigue or creep behaviour and creep-fatigue interaction effects are almost totally unknown.

In this work we report results from tests performed on candidate reduced activation martensitic steels: the F82H mod. and Eurofer 97, both Ta-stabilised, and the Ti-bearing BATMAN IIC and IID. For comparison purposes, two 'conventional' martensitic alloys (MANET II and Grade 91) and the austenitic AISI 316 L(N) steel were also tested under the same conditions.

2. Experimental details

2.1. Testing apparatus

The thermo-mechanical fatigue (TMF) apparatus has been described elsewhere [4–6], but we briefly review the working principles. A hollow cylindrical specimen was chosen to allow fast heating and cooling. The outer and inner diameters of the gauge length are 8 and 4 mm, respectively.

The specimen is rigidly clamped to a closed loop servo mechanical load frame (Mayes Series D); a Lepel/Radyne RF generator performs heating while a forced airflow passing through the loading bars and the specimen provides cooling. Using a relatively low RF frequency (160 kHz for the ferromagnetic materials and 80 kHz for

☆ Work performed in the frame of the European Blanket Project – Structural Materials.
* Corresponding author. Tel.: +39-06 3048 3142; fax: +39-06 3048 4864.
E-mail address: gianni.filacchioni@casaccia.enea.it (G. Filacchioni).

0022-3115/$ - see front matter © 2004 Elsevier B.V. All rights reserved.
doi:10.1016/j.jnucmat.2004.04.057

the 316 SS), we obtained a radial gradient $\leqslant 5$ °C, whereas the longitudinal gradient is limited to ±7 °C.

The 'hot junction' of a K-type thermocouple is flattened and half-wrapped around the sample measuring the gauge length temperature. A Eurotherm 900 unit performs the thermal cycling control; heating–cooling rates from 0.5 to 20 °C/s are possible.

Two side-entry extensometers (50 and 12-mm gauge lengths) are used for elongation measurement or control. The machine load cell measures the applied force. The sensor signals are sent to a central controlling unit, any of these can be used to generate a customised test envelope.

While the possibility of getting compound control (load–temperature, strain–temperature) provides several testing envelopes, the data reported in this work were obtained using the 'self-tuning' thermal fatigue method. These test conditions were already used for a European Round Robin experiment (see Ref. [5]). The sample is submitted to a continuous temperature cycling from T_{min} to T_{max}. The 50-mm gauge-length extensometer defines a constant test zone. With the machine set in extension (strain) control, such that the allowed change in length is zero, the actuator reacts to counterbalance the thermal expansion of the material; in consequence, during the heating phase the sample withstands a compressive load condition while a tensile force develops on cooling. This loading state is commonly known as 'out-of-phase' thermal fatigue.

Then, our test methodology is rather different from those normally used by other laboratories, where tests are carried out by imposing strain boundary conditions to the sample in such a way that the mechanical strain is always supposed to be the opposite of the thermal expansion. So, the thermal fatigue tests are performed by imposing the gauge length deformation to cycle between 0 and $-\alpha \cdot \Delta T$ (a constant strain ratio, R_ε, equal to $-\infty$). That contingency is found in our experiments only during the first half cycle.

The strain or stress response during the remaining part of our test are not independent variables; they are continuously tuned according to the constraint condition imposed by the surrounding, colder, parts of the specimens. These loading conditions are very similar to those of a thick component experiencing cyclic temperature gradients.

2.2. Materials and test parameters

The chemical compositions of materials investigated are summarised in Table 1 [7–11]. Other data regarding their mechanical properties, metallurgical status and microstructure are available in the cited references.

The RAMF materials and Grade 91 specimens were lathe-machined from 25 to 27-mm thick plates, those of the AISI 316 L(N) from a 40-mm thick plate while the MANET samples were manufactured from a 20-mm diameter rod. Surface roughness of the gauge length never exceeded 0.4 μm, the longitudinal hole surface roughness being of the order 2–3.5 μm.

To compare the thermal fatigue behaviour, a temperature range of 400 °C was used; the minimum and maximum temperatures being 200 and 600 °C respectively. Heating and cooling were performed at the same rate of 5 °C/s. No holding times were imposed, the test frequency being of the order of 0.006 Hz.

All specimens were submitted to an initial thermal stabilisation period (10–15 cycles), a null load was imposed all along this time (command set to load control). During that phase the measurement of thermal expansion was carried out. The stabilisation phase also provided a tool for checking the effectiveness of temperature control. At the beginning of the real test, the controlling sensor was switched to the 50-mm gauge length extensometer; no variation on its initial, starting value was allowed. Tests were carried out in air.

Table 1
Chemical composition of steels investigated (% wt)

Alloy	C	Cr	Si	Mn	Ni	Mo	W	V	Nb[a]	Ta	Ti	B[a]	N[a]
BATMAN IIC	0.12	8.67	0.02	0.52	0.02	0.02	1.43	0.2	100	–	0.07	64	57
BATMAN IID	0.13	7.55	0.03	0.52	0.02	0.02	1.41	0.2	100	–	0.07	57	41
F82H mod.	0.09	7.67	0.11	0.16	0.02	0.01	1.96	0.16	1–4	0.04	0.01	10	50
Eurofer 97	0.10	8.87	0.05	0.45	0.028	0.03	1.15	0.2	25	0.14	0.005	10	170
MANET II	0.11	10.3	0.14	0.75	0.65	0.56	–	0.2	1500	–	–	89	300
Grade 91	0.11	8.7	0.24	0.45	0.05	0.9	–	0.19	1000	–	–	74	390
AISI 316 L(N)	0.02	17.34	0.32	1.8	12.5	2.4	–	–	–	–	–	14	800

[a] Amount quantified in ppm.

3. Results

Relevant mechanical quantities are summarised in Table 2. The theoretical hindered thermal strain (THTS) reported in that table is calculated using the formula

$$\mathrm{THTS} = \int_{T_{\min}}^{T_{\max}} \alpha_{\mathrm{inst}}(T)\mathrm{d}T. \quad (1)$$

The instantaneous thermal linear expansion coefficient, $\alpha_{\mathrm{inst}}(T)$, has been calculated from data measured during the thermal stabilisation phase. The $\Delta l/l$ values showed a slightly quadratic dependence on temperature; so, the instantaneous α results in a linear function of the temperature (see Table 3).

Fig. 1 shows an example of stress range and mean stress evolution and clearly illustrates the martensitic steels softening, and how the austenitic alloy strongly hardens. The maximum (tensile) stress value was the quantity used to identify the characteristic number of cycles for each steel. No matter what alloy, any stress–life-time plot shows a central zone in which the stress evolution appears linearly depending on the number of elapsed cycles, in other words $\sigma = A - B \cdot N$. Using a family of parallel lines traced with an 'offset-modified' value of the A coefficient, we can determine the no. of cycles to accommodation, to first crack initiation and finally, identify the life-time to failure. An 'offset' of 1% ($A^* = 1.01$ A) is used by us, conventionally, to represent the end of the accommodation phase N_a (i.e. rearrangement of laths, evolution of fatigue cells and sub cells, slip band development, completion of cyclic hardening or softening). For material showing hardening, this procedure is not applicable; we state that accommodation takes place at the cycle at which the maximum tensile stress is observed.

The number of cycles to initiation (N_{fci}, the onset of macroscopic flaw) is found by tracing a −2.5% offset line ($A^* = 0.975$ A). We considered material failure occurring for a 5% decrease of tensile load ($A^* = 0.95$ A), and this characteristic life-time is identified as $N_{\mathrm{f}(\Delta 5)}$, but $N_{\mathrm{f}(\Delta 25)}$ values have also been reported for a better comparability of results. In fact, the number of cycles corresponding to a 25% decrease in tensile peak stress ($A^* = 0.75$ A), represents a rupture criterion for several authors.

Table 3
Instantaneous linear thermal expansion coefficients $\alpha_{\mathrm{inst}}(T) = A_0 + A_1 \cdot T$

Alloy	A_0	A_1
BATMAN IIC	1.1547×10^{-5}	6.187×10^{-9}
BATMAN IID	1.1733×10^{-5}	5.345×10^{-9}
F82H mod.	1.126×10^{-5}	6.633×10^{-9}
Eurofer 97	1.1203×10^{-5}	5.3204×10^{-9}
MANET II	1.1656×10^{-5}	4.3802×10^{-9}
Grade 91	1.121×10^{-5}	6.032×10^{-9}
AISI 316 L(N)	1.782×10^{-5}	6.151×10^{-9}

Results demonstrated that the most resistant materials are the conventional steels (the MANET II ranking first) followed by the higher Cr Ti-bearing alloy, fourth comes the 316 L(N) and then the remaining Ta- and Ti-stabilised RAFM steels.

SEM analysis showed that fatigue-striation spacing grows from the inner to the outer surface of the specimens and this behaviour was observed in all samples and materials. Initiation sites cannot be exactly located owing to oxidation of the fracture surface, nonetheless, the situation suggests that cracks start and develop from the surface of the central hole, probably owing to the higher surface roughness of that part of the specimen. A full, complete data set, including fractography, is available in Ref. [12].

4. Discussion of results obtained from the TFM campaign

During the first half cycle, the steels show yielding and compressive peak stress occurring well before the maximum temperature has been reached. For martensitic steels we measured plastic strains ranging from

Table 2
Results of TMF comparison tests campaign ($T_{\max} = 600$ °C, $T_{\min} = 200$ °C)

Alloy	N_a	N_{fci}	$N_{\mathrm{f}(\Delta 5)}$	$N_{\mathrm{f}(\Delta 25)}$	$\Delta\sigma$ (MPa)	$\Delta\varepsilon_{\mathrm{tot}}$ (%)	THTS (%)
BATMAN IIC	163 ± 21	584 ± 97	606 ± 102	643 ± 102	597 ± 13	0.5112 ± 0.07	0.5693
BATMAN IID	226 ± 22	764 ± 45	793 ± 101	827 ± 100	587 ± 13	0.527 ± 0.049	0.5673
F82H mod.	157 ± 32	478 ± 88	493 ± 91	516 ± 96	567 ± 5	0.519 ± 0.08	0.5669
Eurofer 97	205 ± 59	598 ± 177	612 ± 181	633 ± 188	577 ± 5	0.5191 ± 0.03	0.54
MANET II	313 ± 13	875 ± 67	905 ± 72	930 ± 76	710 ± 8	0.405 ± 0.04	0.5712
Grade 91	200 ± 10	829 ± 72	866 ± 86	891 ± 88	674 ± 31	0.451 ± 0.007	0.5588
AISI 316 L(N)	154 ± 7	686 ± 191	686 ± 191	700 ± 190	797 ± 7	0.6121 ± 0.08	0.8251

N_a = number of cycles to saturation (achievement of accommodation phase); N_{fci} = number of cycles to crack initiation; $N_{\mathrm{f}(\Delta 5)}$ = number of cycles to failure (Δ5 criterion); $N_{\mathrm{f}(\Delta 25)}$ = number of cycles to failure (Δ25 criterion); $\Delta\sigma$ = stress range; $\Delta\varepsilon_{\mathrm{tot}}$ = total strain range; THTS = theoretical hindered thermal strain (hindered thermal expansion); stress ranges and total strain ranges are half-life ($N_f/2$) values.

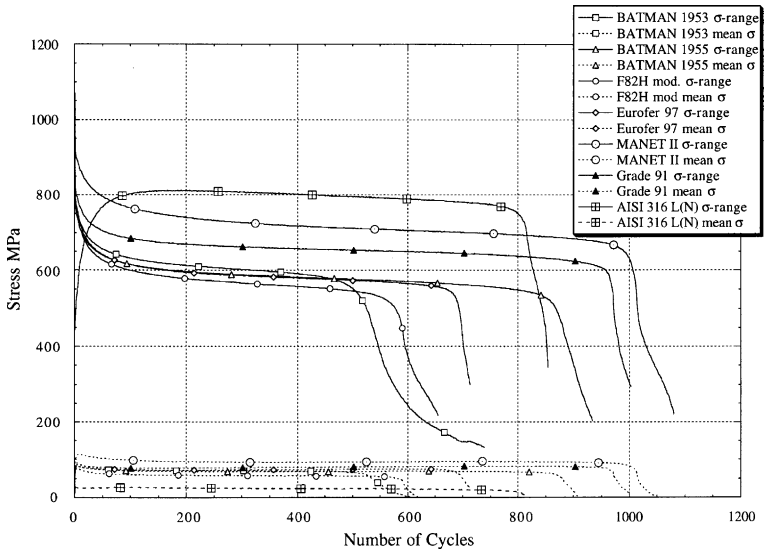

Fig. 1. Evolution of stress range and mean stress as a function of elapsed thermal cycles.

−0.62% to −0.72% after the first heat-up and the temperature corresponding to the maximum compressive stress is in the range 425–445 °C. An even larger deformation is found for 316 L(N), typical values are between −0.92% and −1.3% and a peak compressive stress is observed at 378–395 °C. A large part of the gauge-length shortening is recovered just during the second cycle. An elastic deformation decreases to −0.27%/−0.3% (conventional steel) or to about −0.35%/−0.4% (RAMF alloys). The temperature at which the peak compressive stress occurs increases to 570–580 °C. For the austenitic steel, the inelastic strain shows values around −0.6%/−0.74%, the temperature for the minimum load approximately 595–600 °C.

All martensitic alloys showed a continuous softening, the maximum tensile stress being reached within two to six cycles. Saturation starts beyond 207–392 cycles (N_s/N_f 0.36–0.43) and, as expected, the shorter the accommodation phase, the shorter the life to failure. During that period, the decrease in stress range is within 280–350 MPa; the greatest difference was observed in the conventional steel MANET II while both Ti-bearing alloys showed the smallest difference. In contrast, the 316 L(N) showed an important and protracted hardening, with a tensile peak stress occurring between cycles 140 and 171. The maximum stress range is about 1.88 times that measured in the first cycle.

During saturation, the stress range of all materials decreases with a linear dependence on elapsed thermal cycles. That softening-rate is between 0.046 and 0.07 MPa/cycle for the alloys having the greater Cr content (MANET II, Grade 91, Eurofer 97 and BATMAN IIC) while for the other steels the rate is roughly doubled; −0.095 and 0.11 MPa/cycle, respectively, for BATMAN IID and F82H mod. steel. The corresponding rate for 316 L(N) is 0.07 MPa/cycle.

Regarding the martensitic steels, some characteristic quantities at half-life (like stress range, mean stress and stress ratio) appear to be linearly dependent on the ultimate tensile strength of the material measured at the minimum temperature of the thermal cycle. Moreover, the R_σ-value (the stress ratio) and mean stress of all alloys are remarkably constant during the test until the macroscopic crack (or crack network) commences to propagate.

Once the onset of macroscopic cracking (N_{fci}) occurred, a few tens of cycles (20–40 cycles) are sufficient to achieve a 25% decrease in stress ($N_{f(\Delta 25)}$).

5. Conclusions

The thermal fatigue behaviour of six martensitic steels and one austenitic alloy was compared under continuous thermal cycling from 200 to 600 °C with their thermal expansion totally constrained.

Experimental results showed that:

- The conventional steels are the most TMF-resistant materials.
- Reduced activation martensitic steels having a higher Cr amount behave better than the others. Ti-stabilised steels seem to be more resistant than Ta-alloyed steels. The weakest alloy seems to be the F82H mod.
- In spite of its lower thermal factor, the AISI 316 L(N) demonstrated good resistance. Probably that property is due to its high toughness and the related greater K_{th} and slower stable crack propagation rate.

- All martensitic steels showed a significant softening, whereas the austenitic alloy strongly hardened.
- Cracking always starts and propagates from the axial central hole (owing to a lesser accurate surface finish).

Investigation of thermal fatigue behaviour of fusion relevant structural materials is far from completion. The test matrix has been expanded to introduce others variables like heating–cooling rates and high and low temperature holding times. Thermal fatigue seems to constitute a serious threat to structural integrity, especially if the MFR machine will operate in the creep-sensitive temperature regime.

References

[1] A. Hishinuma, A. Kohyama, R.L. Klueh, D.S. Gelles, W. Dietz, K. Ehrlich, J. Nucl. Mater. 258–263 (1998) 193.
[2] Proceedings of the IEA Working Group Meeting on Reduced Activation Ferritic/Martensitic Steels, Tokyo (J), November 1997.
[3] K. Ehrlich, M. Gasparotto, L. Giancarli, G. Le Marois, S. Malang, B. van der Schaaf, in: European Material Assessment Meeting, EFDA-T-RE-2.0, 2001.
[4] G. Filacchioni, in: Proceedings of Materials for Energy-Efficient Vehicles, 31st ISATA, Düsseldorf (D), June 1998.
[5] G. Filacchioni, C. Petersen, F. Rézaï-Aria, J. Timm: A European Round Robin in Thermo-Mechanical Fatigue Behaviour of a 9%Cr Low Activation Ferrite–Martensite Steel, Thermo-Mechanical Fatigue Behaviour of Materials, vol. 3, ASTM STP 1371, 2000, p. 239.
[6] G. Filacchioni, ENEA Technical Report MAT CMS 003-02, March 2002.
[7] A. Hishinuma, in: Proceedings of the IEA Working Group Meeting on Ferritic/Martensitic Steels, Sun Valley, USA, 24 June 1994.
[8] L. Pilloni, F. Attura, A. Calza-Bini, G. De Santis, G. Filacchioni, A. Carosi, S. Amato, J. Nucl. Mater. 258–263 (1998) 1329.
[9] G. Filacchioni, E. Casagrande, U. De Angelis, ENEA Internal Report, 1995, not published.
[10] G. Filacchioni, E. Casagrande, U. De Angelis, G. De Santis, D. Ferrara, L. Pilloni, J. Nucl. Mater. 271–272 (1999) 445.
[11] M. Shirra, P. Graf, S. Heger, H. Meinzer, W. Schweiger, H. Zimmermann, KfK Internal Report, 1993, KfK 5177.
[12] G. Filacchioni, E. Casagrande, U. De Angelis, G. De Santis, D. Ferrara, ENEA Technical Report MAT CMS 004-02, November 2002.